IET Journals
The Institution of Engineering and Technology

Resilience-Oriented Restoration in Modern Power Distribution Networks With Smart Electric Vehicles Coordination Framework

ISSN 1751-8644
doi: 0000000000
www.ietdl.org

Abdullah Ali M Alghamdi[1,2*], *Dilan Jayaweera*[1]

[1] *Electronic, Electrical and Systems Engineering, School of Engineering, University of Birmingham, Birmingham, UK*
[2] *Electric Engineering, School of Engineering, Taibah university, Medina, KSA*
** E-mail: axa1455@bham.ac.uk*

Abstract: In the era of cyber-physical-social systems, research lacks a comprehensive framework to optimize dynamic coordination strategies for electric vehicles (EVs) to enhance modern power distribution networks (MPDNs) resilience. Public studies have not comprehensively addressed the impact of intelligent transportation systems (ITS) and smart charging systems (SCS) on MPDN resilience strategies after rare events. To bridge this gap, a two-stage EVs coordination framework is proposed to consider MPDN smart restoration. The first stage involves a novel proactive EV prepositioning model to optimize EV prepositioning plans before a rare event in order to enhance MPDN survivability during the immediate aftermath of the event. The second stage involves an advanced spatial-temporal EV dispatching model to maximize the number of available EVs for discharge, thereby improving MPDN recovery after a rare event. The proposed framework includes an information system facilitating dynamic data exchange between EVs and ITS/SCS automated systems and introduces a novel geographic graph to optimize EV routes between charging points. Effectiveness of the framework is assessed on a modified IEEE 123 node test feeder incorporating real-world transportation and charging infrastructure. The results suggest that significant enhancement in MPDN resilience is possible with smart restoration strategies. Sensitivity analysis specifically demonstrates that integrating recently invented technologies of the smart charging systems and automated systems potentially provides significant benefits if dynamic coordination strategies are employed in MPDNs.

Nomenclature

Indices

β, ζ	Indices for longitude
γ, δ	Indices for latitude
ϕ	Index for phase number
ρ, ϱ	Indices for two end of the proposed graph segments
av, tr	Indices for the availability and travelling status
B, N	Indices for line and node
C, O	Indices for capacitor and lines in a loop
ch	Index for the charging status
CP, cp	Indices for charging point
D, U	Indices for diversified and undiversified load
$disch$	Index for the discharging status
E, e	Indices for electric vehicle
F, S	Indices for faulty, and switchable component
i, j, ij	Indices for two end nodes and line
R, r	Indices for road
RCS	Index for remotely-switchable component
t, l	Indices for time and load
V, L	Indices for components associated with voltage regulators and loads

Sets

$\check{\mathcal{Y}}$	Set of vertices indicate electric vehicle coordinates
$\widehat{\mathcal{Y}}$	Set of vertices indicate charging point coordinates
$\mathcal{H}$	Set of the proposed graph including intersections and edges
$\mathcal{K}, \mathcal{E}$	Set of intersections and edges of the proposed graph
$\mathcal{N}, \mathcal{B}$	Set of nodes and lines
$\mathcal{R}, \mathcal{Y}$	Set of segments and vertices in a road map
$\mathcal{T}, \mathcal{G}$	Set of time intervals and electric vehicles
$\mathcal{V}, \mathcal{C}$	Set of voltage regulators and capacitors
$\mathcal{Z}$	Set of road map including segments and vertices
$\Phi, \mathcal{L}$	Set of phases and loads

Decision Variables

$CR^{R}_{r,t}$	Congestion rate of road r at time t
$D_{e,cp,r,t}$	Sum of travelling distance on road r between electric vehicle e and cp
$D_{k_\varrho,k_\rho,e,t}$	Sum of travelled distance for electric vehicle e at time t
$P^{ch/disch}_{e,t}$	The charging/discharging active power for electric vehicle e at time t
$Q/P_{i,\phi,t}$	The three phase reactive/active power for node i at time t
$Q/P_{l,\phi,t}$	The three phase reactive/active power for load l at time t
$Q/P^{D}_{l,\phi,t}$	The three phase diversified reactive/active power for load l at time t
$Q/P^{U}_{l,\phi,t}$	The three phase undiversified reactive/active power for load l at time t
$S/Q/P_{ij,\phi,t}$	The three phase apparent/reactive/active power from node i to node j at time t
$SOC^{av}_{e,t}$	Available stat-of-charge level for electric vehicle e at time t
$SOC^{tr}_{e,t}$	Consumed stat-of-charge during travelling for electric vehicle e at time t
$t^{tr}_{e,r}$	Total travelling time of electric vehicle e on road r
$V_{i,\phi,t}$	The three phase voltage magnitude for node i at time t
$x_{cp,t}$	Binary variable equals 1 if charging point cp is operational at time t
$x_{e,cp,t}$	Binary variable equals 1 if electric vehicle ev is connected to a charging point cp at time t
$x_{e,t}$	Binary variable equals 1 if electric vehicle ev is connected at time t
$x^{ch/disch}_{e,t}$	Binary variable equals 1 if electric vehicle e at time t
$x_{i,\phi,t}$	Binary variable equals 1 if phase ϕ in node i is connected at time t
$x_{ij,\phi,t}$	Binary variable equals 1 if phase ϕ in line ij is connected at time t
$x_{k_\varrho,k_\rho,e,t}$	Binary variable equals 1 if electric vehicle e travels between k_ϱ and k_ρ at time t
$x_{l,t}$	Binary variable equals 1 if load l is connected at time t
$x_{v,\phi,t}$	Binary variable equals 1 if phase ϕ in line with voltage regulator v is connected at time t

1 Introduction

Electric vehicles (EVs) play a crucial role in enhancing modern power distribution networks (MPDNs) resilience as mobile power sources due to their ability to move over transportation systems and use distributed smart charging points [1, 2]; particularly, in areas with a high penetration of EVs and sufficient charging points [2, 3]. The utilization of different types of emergency mobile power sources (EMPSs) have been studied in the literature for resiliency-oriented restoration strategies to support MPDN outage load. The authors propose a two-stage restoration scheme for enhancing distribution system resilience during emergencies, like seismic disasters. It involves optimizing MPS routing and scheduling, along with dynamic network reconfiguration. In [4], a two-stage restoration scheme is proposed to enhance the resilience of MPDNs during emergencies. The routing and scheduling of EMPSs are optimised in coordination with dynamic network reconfiguration. However, the practical deployment and coordination of EMPSs may face challenges, such as limited power availability and inadequate charging infrastructure for EVs. In [5], a dynamic load restoration method is proposed to restore service in MPDNs effectively by considering the interdependence with the transportation system. However, the assumption of uniformity among mobile generators may not always hold true, which can impact the effectiveness of the method. Therefore, additional testing and refinement are necessary before implementing this method in real-world scenarios. In [6], a time-space network is utilized to optimize the routing of flexible EMPSs for MPDN restoration, enhancing calculation efficiency. A transportation network simplification method is proposed to reduce the number of binary variables involved in the optimization process. However, the absence of implemented charging infrastructures for mobile energy storage power sources adds additional complexity to the transportation network simplification method, requiring more nodes and binary variables. In [7–9], a joint restoration model is suggested to enhance post-disaster resilience by coordinating electric bus scheduling and MPDNs restoration. The model focuses on maximizing load pickups and minimizing electric bus rental expenses. However, it should be noted that the assumptions of charging station availability and bus companies' willingness to participate may not accurately represent real-world implementation. In [10, 11], a rolling optimization framework for MESSs is proposed. It can effectively optimize the allocation and scheduling of MESSs, microgrids, and MPDN reconfiguration to restore critical loads during extreme events. However, the proposed approach simplifies the distribution network and transportation network models, neglecting the real-world constraints of movement of mobile power sources such as charging points availability and road closures.

1.1 Motivation

In the aforementioned literature, the utilised EMPSs are limited by their utility and rely on prior knowledge of the outage and the affected area. They may not be sufficient for unexpected outages or larger affected areas, resulting in extended outages and disruptions. Furthermore, the lack of an intelligent coordination framework for EVs with high penetrations leads to inefficient resource use, and increased EV penetration complicates transportation and charging station automated system prepositioning plans and dispatching strategies, necessitating more sophisticated and smart restoration strategies to ensure EVs access charging stations efficiently and without causing further disruptions.

Henceforward, an ingenious framework for coordinating EVs is requisite to enhance MPDN resilience, so as to effectively manage the massive data generated by the motion and information production of EVs. This can be achieved by the integration of MPDN, smart charging system (SCS), and intelligent transportation systems (ITS) [1, 12, 13]. The Internet of Things (IoT) and fifth-generation (5G) network technologies expedite the communication between ITS/SCS automated system and EVs for coordination throughout recently invented machinery that facilitates vehicular communications like roadside unit (RSU) and charging points with vehicle-to-everything (V2X) operation mode [14, 15]. Incorporating these technologies enables ITS/SCS automated system and MPDN operator to store the information of EVs, roads, and charging points across distributed data centres (DDCs) and simultaneously update resilience-oriented restoration plans of roads, charging points, and MPDN components in real-time [16]. The advent of cyber-physical social systems has facilitated data exchange of EVs through efficient information system [17, 18], where this capability is particularly relevant for MPDN restoration and is considered desirable by power utilities seeking to improve MPDN resilience in the face of high impact low probability events (i.e., rare events).

On the other hand, rare events can destroy transportation system roads and charging points which in turn impact the dispatching of EVs and impose more challenges to service restoration for enhancing MPDN resilience. Commonly, the literature focuses on coupling MPDN branches and transportation roads for emergency mobile power source dispatching problems but neglects geographic factors like actual locations, travel distance, energy consumption rates, road congestion and damage status, as well as charging points capacity, characteristics, and technology. Although there has been progress in deploying transportation roads constraints in [5, 10, 19], current research studies on dispatching problems consider transportation and charging station systems in a deterministic manner or do not thoroughly consider the full impact of interrelated geographic and spatial-temporal positioning and dispatching constraints on the intelligent transportation system and smart charging system for enhancing MPDN resilience after a rare event.

1.2 Major Contributions

To address the aforementioned challenges and further enhance MPDN resilience, an innovative resilient EVs coordination framework with a novel proactive prepositioning model and an advanced spatial-temporal dispatching model is proposed in this paper to effectively bridge the coordination gap in the large penetration of EVs.

A novel communication methodology is also proposed for exchanging EVs data to further enhance MPDN resilience, which takes into account the automated system of the intelligent transportation system (ITS) and smart charging system (SCS). The methodology uses real traffic data and patterns for simulating a typical EV driving behaviour in a the real world.

Further, a novel bidirectional geographic graph is proposed to consider spatiotemporal factors such as actual distance, traffic conditions, charging station availability, and power demand to optimize the routes between charging points and EVs accordingly. This helps to reduce the load on the SCS and prevent overloading and queuing, which can cause power outages and other disruptions.

The paper is structured as follows: Section 2 presents the problem statement and the proposed information system. Section 3 provides the mathematical formulation. Section 4 covers the solution method and linearizations. Section 5 presents the simulation studies and results, as well as the sensitivity analysis. Section 6 provides further remarks of the proposed work. Section 7 concludes this article. Section 9 presents the appendices.

2 EVs Coordination Framework

2.1 Problem Statement

A modified conceptual resilience curve (R) is presented in Fig. 1, to illustrate the variance in MPDN robustness level during the pre-disruption ($t_0 \sim t_e$), disruption progress ($t_e \sim t_{pe}$), and restorative phases ($t_{pe} \sim t_{pr}$) of a rare event [20]. The dashed line represents the results obtained from the proposed method, while the solid line represents the conventional approach. The comparison is shown to highlight the superiority of the proposed method. The paper employs two categories of measures to enhance resilience: planning-oriented measures before the event ($t_0 \sim t_e$) in the first stage, and operation-oriented measures after the event ($t_{pe} \sim t_{pr}$) in the second stage.

In the first stage, the MPDN survivability is evaluated from t_{pe} to t_r, which proves the ability of the proposed EVs propositioning model to enhance the MPDN resilience from R_r to R'_r at an earlier time (t'_r) which is earlier than t_r. The MPDN reconfiguration model is co-optimized to shift the system into a state of less impacted and stressed by the event [21].

In the second stage, the MPDN recovery is measured from t_r to t_{pir} proving the capability of the proposed EVs dispatching model to enhance the MPDN resilience from R_{pr} to R'_{pr} and achieves complete restoration at t'_{pir} enhancing MPDN robustness level from (R_0) to (R'_0). Spatiotemporal routing and dynamic power scheduling of EVs, dynamic network reconfiguration and dynamic power dispatch of the MPDN, are co-optimized in this stage. As a result, the proposed EVs coordination framework enhances the MPDN resilience from the solid curve, in Fig. 1, to the dashed curve.

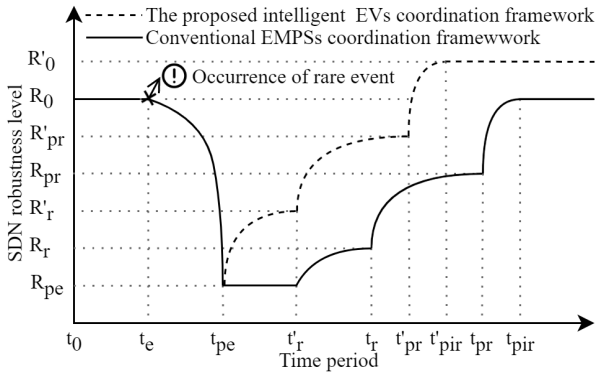

Fig. 1: A modified conceptual resilience curve associated with an event [20]. The comparison is shown to highlight the superiority of the proposed intelligent EVs coordination framework (i.e., dashed line) over the conventional EMPSs coordination framework (i.e., solid line).

2.2 Algorithm

The innovative algorithm in this section is proposed to maintain EVs and charging points (CPs) do not deviate from their prepositioning and dispatching plans obtained by ITS/SCS automated system and MPDN operators via the proposed information system in Section 2.3. These are achieved by modelling binary variables ($x_{e,t}$), ($x_{cp,t}$), and ($x_{e,cp,t}$), in which they are explained in this section, respectively.

For the former variable ($x_{e,t}$), EVs are categorised based on their connection mode. First, away EV (A-EV) which refers to EV cannot participate in the restoration processes due to it is connected to unidirectional CP, and/or its state-of-charge level (SOC_e) is equal or lower than the minimum value ($\underline{SOC_e}$). Here, $x_{e,t} = 0 \forall t$. Second, connected EV (C-EV) refers to EV that can participate in the restoration process since it is connected to bidirectional CP and its SOC_e is greater than $\underline{SOC_e}$. Here, $x_{e,t} = 1 \forall t \Rightarrow SOC_e \geq \underline{SOC_e}$. Third travelling EV (T-EV) which to EV that is travelling and cannot connect until arriving time ($t^{ar}_{e,cp}$) is reached, where $t = t^{ar}_{e,cp}$. To enable participation in this category, T-EV calculated SOC_e at $t^{ar}_{e,cp}$ must be greater than $\underline{SOC_e}$. Here, $x_{e,t} = 1, t \geq t^{ar}_{e,cp} \Rightarrow SOC_e \geq \underline{SOC_e}$.

For the medial variable ($x_{cp,t}$), CPs are classified based on their technologies into two categories. First, bidirectional charging point (V2G-CP) which is a CP support vehicle-to-grid (V2G) operation mode, for example, Vehicle-to-building (V2B) operation mode, which can inject the power to the MPDN allowing C-EV to discharge. Various capacities (i.e., the characteristics of supplying electric power to an EV, ranging from slow to ultra-rapid), and capabilities (i.e., the constraint of charging slot allows for connection to only one EV at each time period ($t_n \sim t_{n+\tau}$), given τ is the connection period of time). Here, $x_{cp,t} = 1 \forall t$ if it is not damaged, and 0 otherwise. Second, a unidirectional charging point (V1G-CP) that is a CP cannot inject the power back to the MPDN, for example, in vehicle-to-home (V2H) operation mode. Here, $x_{cp,t} = 0 \forall t$.

For the latter variable ($x_{e,cp,t}$), if a C-EV is connected to V2G-CP, it is equal to 1 for the connection period ($t^{ar}_{e,cp} \leq t \leq \tau$), and 0 otherwise. As a result, charging/discharging processes, connecting and disconnecting timings, and routes and destinations comply with the obtained EVs prepositioning and dispatching plan of the ITS/SCS automated system.

2.3 Information System

The data obtained by the ITS/SCS automated system in the first and second stages are automatically transmitted to distributed data centres (DDCs) via roadside units (RSUs) of intelligent transportation infrastructure [22]. Thus, MPDN operators and ITS/SCS automated system dynamically update the MPDN resilience-oriented restoration plan at each predefined time step. Moreover, ITS/SCS automated system share data with EVs throughout vehicle-to-everything (V2X) mode of operation [23]; particularly, vehicle-to-infrastructure (V2I) communications [24].

In the first stage, the MPDN operator and the automated system of the intelligent transportation system (ITS) and smart charging system (SCS) take preventive actions to enhance MPDN resilience. Particularly, SCS automated system collects the technical and geolocation information of V2G-CPs and C-EVs to maximise the available EVs aftermath, allowing them to participate and discharge shortly after the rare event. Meanwhile, the MPDN operator maximises the survived loads while maintaining the constraint of their network's components. At the same time, ITS automated system plans for the restorative phase by collecting locations and technical data of T-EVs, which are used to optimize the critical route for each EV once the road damage status and traffic conditions are obtained shortly after the event. For example, as in Fig. 2(a), SCS automated system collects technical data of V2G-CPs, C-EV6, and C-EV5, while T-EV1 and T-EV2 are prepositioned. Note that, T-EV3 is not eligible due to its low $SOC^{av}_{e,t}$ level.

In the second stage, the restorative actions are taken based on the preparation actions in the first stage. Specifically, SCS automated system reports the V2G-CPs damage status and updates the available energy of C-EVs ($SOC^{av}_{e,t}$). This is achieved in accordance with ensuring C-EVs are immediately disconnected if their SOC_e level reaches the minimum boundary ($\underline{SOC_e}$), allowing the next T-EV in the queue to participate immediately avoiding long queues, as well as, to maximise the use of charging points. Meanwhile, the ITS automated system updates traffic data, road status, and congestion rate at each time step to dynamically optimise the critical path for T-EVs. Meantime, the MPDN operator updates the network components' status based on the provided reports by repair crews (RCs). For instance, Fig. 2(b) shows C-EV6 is disconnected so that T-EV2 can connect and discharge, ITS automated system shares optimal routes between V2G-CPs and T-EV1 and T-EV2, while C-EV5 is discharging.

3 Mathematical Formulation

3.1 Proactive Prepositioning of EVs

Before a rare event, MPDN operator and ITS/SCS automated system collaborate to maximize the number of connected EVs for enhancing MPDN survivability. The objective function of the first stage, in (1), maximizes the amount of survived MPDN loads at $t = 0$.

$$\min_{e,cp,t} (\max_{l,\phi,t} \sum_{t} \sum_{l} \sum_{\phi} [x^L_{l,t} \cdot P^L_{l,\phi,t}]) \quad (1)$$
$$, \forall l \in \mathcal{L} \subset \mathcal{K}, e \in \breve{\mathcal{Y}} \subset \mathcal{K}, cp \in \widehat{\mathcal{Y}} \subset \mathcal{K}, \phi \in \Phi, t = 0$$

Unlike [4, 5, 7–11, 19, 25–31], the number of available EVs is not predetermined here. Thus, the objective function facilitates the prompt discharge of available EVs following the event to maximise

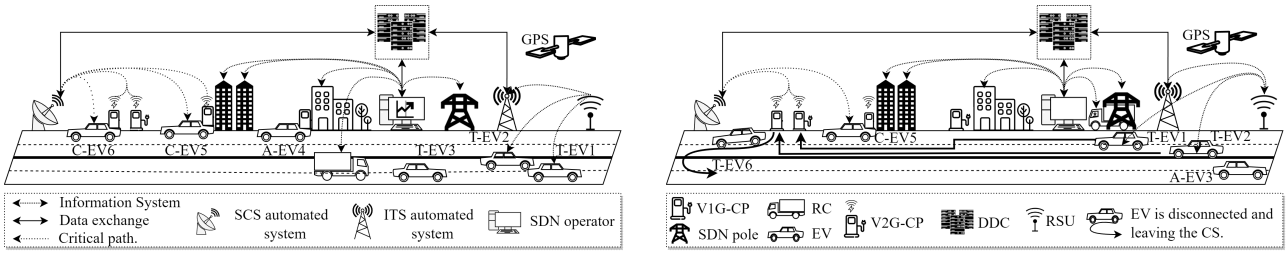

Fig. 2: An illustration of the proposed EVs coordination framework. (a) The preventive actions associated with the first stage (before the event $[t_0 \sim t_{pe}]$). (b) The restorative actions associated with the second stage (after the event $[t_{pe} \sim t_{pr}]$).

the amount of restored load in the inner level, while obviating the necessity for further EV discharge if all loads are survived in the outer level. Involved the variables in the outer level, constraint (2) is modelled using the charging status ($x_{e,t}^{ch}$) and discharging status ($x_{e,t}^{disch}$) binary variables to ensure EVs are prepositioned and connected at predetermined CPs to start discharging immediately after the event. Constraint (3) maintains the capability of charging point/station.

$$x_{e,t}^{ch} + x_{e,t}^{disch} \leq x_{e,cp,t}, \forall e \in \mathcal{G}^E, cp \in \mathcal{N}^{CP}, t = 0 \quad (2)$$

$$\sum_{e} x_{e,t} \leq x_{cp,t}, \forall e \in \mathcal{G}^E, cp \in \mathcal{N}^{CP}, t = 0 \quad (3)$$

The problem of prepositioning is intelligently addressed by utilizing the variables that are interrelated with the second stage making the proposed approach novel and highly effective for improving MPDN resilience. This is due to several reasons. First, the approach effectively incorporates the diverse categories of EVs and CPs in the proposed algorithms in Section 2.2. In addition, the information system outlined in Section 2.3 for well-coordination between the MPDN operators and ITS/SCS automated system is effectively pursued. Accordingly, the proposed method ensures the continuous development of MPDN resilience. The inner level of the objective function is subjected to the following constraints:

$$\begin{aligned} &V_{i,\phi,t} - V_{j,\phi,t} \leq \widetilde{z}_{ij,\phi} S_{ij,\phi,t}^{*} + \widetilde{z}_{ij,\phi}^{*} S_{ij,\phi,t} \\ &+M\left(1 - x_{i,\phi,t}^{N}\right), \forall ij \in \mathcal{B}/\mathcal{V}, \phi \in \Phi, t = 0 \end{aligned} \quad (4)$$

$$\begin{aligned} &V_{i,\phi,t} - V_{j,\phi,t} \geq \widetilde{z}_{ij,\phi} S_{ij,\phi,t}^{*} + \widetilde{z}_{ij,\phi}^{*} S_{ij,\phi,t} \\ &-M\left(1 - x_{i,\phi,t}^{N}\right), \forall ij \in \mathcal{B}/\mathcal{V}, \phi \in \Phi, t = 0 \end{aligned} \quad (5)$$

$$\begin{aligned} &\left(\underline{V}_{i,\phi,t}\right)^2 V_{i,\phi,t} \leq V_{j,\phi,t} \leq \left(\overline{V}_{i,\phi,t}\right)^2 V_{i,\phi,t} \\ &, \forall i,j \in \mathcal{V}, \phi \in \Phi, t = 0 \end{aligned} \quad (6)$$

$$\begin{aligned} &\sum_{ji} P_{ji,\phi,t}^{B} + P_{e,\phi,t}^{disch} = \sum_{ij} P_{ij,\phi,t}^{B} + P_{e,\phi,t}^{ch} + P_{l,\phi,t}^{L} \\ &, \forall e \in \mathcal{G}^E, \phi \in \Phi, t = 0 \end{aligned} \quad (7)$$

$$\begin{aligned} &\sum_{ji} Q_{ji,\phi,t}^{B} + Q_{e,\phi,t}^{disch} + Q_{v,\phi,t}^{C} = \sum_{ij} Q_{ij,\phi,t}^{B} + Q_{l,\phi,t}^{L} \\ &, \forall e \in \mathcal{G}^E, \phi \in \Phi, v \in \mathcal{V}, t = 0 \end{aligned} \quad (8)$$

The three-phase unbalanced power flow model is applied here since the MPDN is naturally unbalanced [32–35]. First, constraints (4)-(5) represent the three-phase line model that ensures the feasible range of voltage difference between two end nodes (i), and (j), of each line (i,j) and phase (ϕ) except voltage regulators and transformers. Note, $\widetilde{z}_{ij,\phi} \in \mathbb{C}^{3\times3}$ is the equivalent three-phase line impedance matrix consisting of constant values defined in [33]. The three-phase apparent power ($S_{ij,\phi,t}$) from node (i) to node (j) at time (t) is equivalent to $\left[P_{ij,a,t} + \mathrm{i}Q_{ij,a,t}, P_{ij,b,t} + \mathrm{i}Q_{ij,b,t}, P_{ij,c,t} + \mathrm{i}Q_{ij,c,t}\right] \in \mathbb{C}^{3\times3}$. Note that, subscript "$i$" denotes the node index, while a complex number of the imaginary part is denoted as "i". M is a large positive number and it is selected to ensure the constraints are valid only when the line is energized. Second, the regulators are assumed to be wye-connected and the tap setting is continuous [36] and approximated as suggested in [37] using constraint (6) forcing the regulators' voltage on the secondary side of the voltage regulator to be within 5% of the primary side. Constraints (7)-(8) are three-phase active and reactive power node balance, respectively.

Furthermore, the mathematical formulations of the remaining MPDN operational constraints are presented in the Appendices Section of the paper (Section 9.1) as in equations (20)-(25). These include the radiality constraint, active power limits for EV charging and discharging operations, limits on capacitor reactive power, and the limits of line power, node voltages, and regulator voltages.

3.2 Dynamic Dispatch of EVs

After the occurrence of a rare event, the damage to MPDN components is addressed by the MPDN operator, at the same time, ITS/SCS automated system report the status of roads and charging points, respectively. In this stage, large penetration of EVs is dispatched aiming to restore the maximum amount of outage MPDN loads as follows:

$$\begin{aligned} &\max \sum_{t} \Big(\sum_{\phi} \sum_{l} [x_{l,t}^{L} \cdot P_{l,\phi,t}^{L}] \\ &- \sum_{cp} \sum_{e} \sum_{r} [D_{e,cp,r,t} \cdot ECR_e]\Big) \\ &, \forall l \in \mathcal{L} \subset \mathcal{K}, e \in \breve{\mathcal{Y}} \subset \mathcal{K}, cp \in \widehat{\mathcal{Y}} \subset \mathcal{K}, r \in \mathcal{R} \subset \mathcal{E}, \\ &\phi \in \Phi, t \in \mathcal{T} \end{aligned} \quad (9)$$

In (9), the first line maximizes the amount of restored loads, ensuring that each load is restored non-decreasingly and fully recovered, which prevents the restored load from being shed again. The second line minimizes the energy used in the transportation of EVs, taking into account the energy consumption rate (ECR_e) and considering only critical routes to avoid unnecessary travel of EVs, which results in additional deficit energy. The objective function quantifies MPDN resilience via optimal EVs routing and power scheduling maintaining MPDN operational constraints, which they presented in the following subsections, respectively.

3.2.1 Spatial-temporal routing model:

Considering transportation system geographic constraints, the road map is defined by a bidirectional geographic graph ($\mathcal{Z}(\mathcal{Y},\mathcal{R})$). For intersections set ($\mathcal{Y}$), each node ($y:(\gamma,\beta)$) is determined by its coordinate (i.e., longitude (γ) and latitude (β)). This set contains the coordinates of charging points ($\widehat{y}:(\gamma,\beta) \in \widehat{\mathcal{Y}}$), and EVs ($\breve{y}:(\gamma,\beta) \in \breve{\mathcal{Y}}$). On the other hand, ends of road (r) in the set of edges ($\mathcal{R}$) are modeled as $(y_\delta, y_\zeta) \in \mathcal{R}$. Similarly, the MPDN is designed as a bidirectional geographic graph ($\mathcal{G}(\mathcal{N},\mathcal{B})$). In the set of buses ($\mathcal{N}$) nodes are indexed by $i:(\gamma_i,\beta_i)$, and $j:(\gamma_j,\beta_j)$, and branches are indicated as $\mathcal{B}$=$\{(i:(\gamma_i,\beta_i), j:(\gamma_j,\beta_j))|i,j \in \mathcal{N}; i \neq j\}$. Correspondingly, the aforementioned graphs are combined into the proposed bidirectional geographic graph ($\mathcal{H}$) with a set of nodes

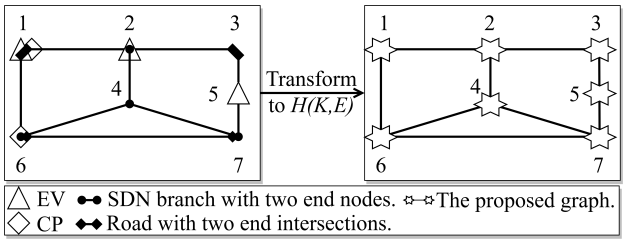

Fig. 3: An illustration the proposed geographic graphs $\mathcal{H}(\mathcal{K},\mathcal{E})$.

($\mathcal{K}$) and edges ($\mathcal{E}$). For the set of nodes/intersections ($\mathcal{K}$), the geographic graph ($\mathcal{H}$) is intelligently modelled to reduce the overall number of nodes without losing any associated coordinates. Accordingly, similar coordinates are merged which in turn significantly reduces the overall computational burdens for the proposed methodology. For example, two graphs are represented in Fig. 3 demonstrating the aforementioned graphs and the proposed geographic graph. The number of intersections at $node1$ is four (i.e., an EV, a CP, and the ends of two roads). However, these four intersections are merged to become one node in $\mathcal{H}(\mathcal{K},\mathcal{E})$. For the set of edges/segments ($\mathcal{E}$), combining the aforementioned graphs into the proposed graph increases the segments of the associated edges ($\mathcal{E}$=$\{(k_\rho, k_\varrho)|k_\rho, k_\varrho \in \mathcal{K}; \rho \neq \varrho\}$), which in turns will increase the accuracy of calculating the actual distance between EVs and CPs. For instance, the edge ($k_3 \sim k_7$) in Fig. 3 has become two segment (i.e., $k_3 \sim k_5$, and $k_5 \sim k_7$).

Consequently, the proposed routing model not only exhibits advanced geographical capabilities that facilitate coordinating large penetration of EVs across roads and CPs but also includes a dynamic update of a large volume of EVs data that permits movement in multiple directions. This is achieved by introducing a bidirectional flow variable ($\overleftrightarrow{x}^R_{k\rho,k_\varrho,e,t}$), which allows each EV to travel between node k_ϱ and node k_ρ in either direction mimicking the typical EV driving behaviour in the real world. To ensure precise computation of the critical distance traveled by an EV (e) and its associated charging point (cp), constraint (10) is introduced. This constraint represents a nonlinear model that calculates the critical path distance ($D_{k_\varrho,k_\rho,e,t}$) accurately.

$$D_{k_\rho,e,t} = \sum_{k_\varrho} x_{k_\varrho,k_\rho,e,t}(D_{k_\varrho,e,t} + (D_{k_\varrho,k_\rho,e,t}x^{tr}_{e,t}CR^R_{r,t})) \\ ,\forall(k_\varrho,k_\rho) \in \mathcal{K}, (k_\varrho,k_\rho) : (\gamma,\beta) = \breve{y} : (\gamma,\beta) \\ ,e \in \mathcal{G}^E, t \in \mathcal{T}, t+\tau \leq \mathcal{T}, \tau \leq t^{tr}_{e,r}, r \in \mathcal{E} \tag{10}$$

The rest of the mathematical formulation of the proposed routing model is provided in the Appendices Section of the paper (Section 9.2) as in equations (26)-(29). These equations upholds routing constraints to ensure compliance with the EVs' routing plan, maintain the designated start and end intersections, enforce the required travel distance for EVs, eliminate sub-tours, and calculate the critical path distance for each EV.

3.2.2 *Dynamic power scheduling model:*

Practically, the amount of energy consumed ($SOC^{tr}_{e,t}$) by an EV (e) during travelling is relatively small. However, the proposed framework coordinates a large number of EVs, so the cumulative amount of $SOC^{tr}_{e,t}$ is considerable and affects the resilience-oriented restoration strategy; hence, constraint (11) is used to calculates the available SOC level of EVs.

$$SOC^{av}_{e,t} = SOC^{av}_{e,t-1} + (\eta^{CH}P^{ch}_{e,t} - \frac{P^{disch}_{e,t}}{\eta^{disch}})\Delta t \\ -SOC^{tr}_{e,t}, \forall e \in \mathcal{G}^E, r \in \mathcal{R}, t \in \mathcal{T} \tag{11}$$

Constraint (12) is a nonlinear model computes the energy consumption during travelling on critical routes ($SOC^{tr}_{e,t}$) considering the energy consumption rate (ECR_e) for each EV (e) individually.

$$SOC^{tr}_{e,t} = x^{tr}_{e,t}ECR_eD_{k_\varrho,k_\rho,e,t} \\ ,\forall e \in \mathcal{G}^E, t \leq t^{ar}, k_\varrho, k_\rho \in \mathcal{K}, k_\varrho : (\gamma,\beta) = \breve{y} : (\gamma,\beta), \\ k_\rho : (\gamma,\beta) = \widehat{y} : (\gamma,\beta) \tag{12}$$

Also, constraints (30)-(36) in the Appendices Section (Section 9.3) are formulated to ensure EVs adhere to the obtained scheduling plan of the ITS/SCS automated system. Accordingly, this model includes constraints that limit the SOC level of EVs, active power limits for EVs, exclusive charging and discharging actions, CP capability and connection maintenance, and capacity control for charging demand and the power injected to the grid during EV discharging operations..

3.2.3 *Modern Power Distribution Network Operational Constraints:*

After an extended period of outage, the effect of the cold load pickup (CLPU) phenomenon may happen [38], considering the diversified load (P^D_L), and undiversified load (P^U_L). The CLPU constraint for active and reactive power are formulated as in constraints (13)-(14), as per [37, 39].

$$P^L_{l,\phi,t} = x^L_{l,\phi,t}P^D_{l,\phi,t} + \left(x^L_{l,\phi,t} - x^L_{l,\phi,t-1}\right)P^U_{l,\phi,t} \\ ,\forall\phi \in \Phi, l \in \mathcal{L}, t \in \mathcal{T} \tag{13}$$

$$Q^L_{l,\phi,t} = x^L_{l,\phi,t}Q^D_{l,\phi,t} + \left(x^L_{l,\phi,t} - x^L_{l,\phi,t-1}\right)Q^U_{l,\phi,t} \\ ,\forall\phi \in \Phi, i \in \mathcal{L}, t \in \mathcal{T} \tag{14}$$

Considering a modern power distribution network, the set of switchable loads ($\mathcal{L}^S$) and non-switchable loads ($\mathcal{L}/\left\{\mathcal{L}^S\right\}$) are modelled. A non-switchable load (l) is energized immediately if it is connected to an energized node (i) using constraint (15), on the other hand, constraint (16) requires the switchable loads (l) can only be energized if it is connected to an energized node (i). Constraint (17) ensures loads ($\mathcal{L}$) are not tripped again after they have been restored.

$$x^L_{l,t} = x^N_{i,t}, \forall l \in \mathcal{L}/\left\{\mathcal{L}^S \cup \mathcal{L}^F\right\}, \phi \in \Phi, t \in \mathcal{T} \tag{15}$$

$$x^L_{l,t} \leq x^N_{i,t}, \forall l \in \mathcal{L}^S/\mathcal{L}^F, \phi \in \Phi, t \in \mathcal{T} \tag{16}$$

$$x^L_{l,t} - x^L_{l,t-1} \geq 0, \forall l \in \mathcal{L}^S, \phi \in \Phi, t \in \mathcal{T} \tag{17}$$

Remotely controlled switches (RCSs) are considered with manual switches in the MPDN. Constraints (18)-(19) limit the number of switching operations which are expressed by the binary variable ($x^{RCS}_{ij,\phi,t}$). It is equal to 1 if the line switches its status from 0 (off) to 1 (on), or from 1 (on) to 0 (off).

$$x^{RCS}_{ij,\phi,t} \leq x^B_{ij,\phi,t} - x^B_{ij,\phi,t-1}, \forall ij \in \mathcal{B}^S, \phi \in \Phi, t \in \mathcal{T} \tag{18}$$

$$x^{RCS}_{ij,\phi,t} \leq x^B_{ij,\phi,t-1} - x^B_{ij,\phi,t}, \forall ij \in \mathcal{B}^S, \phi \in \Phi, t \in \mathcal{T} \tag{19}$$

Also, the fault location, isolation, and service restoration (FLISR) model is integrated and represented in the Appendices Section (Section 9.4), specifically captured by constraints (37)-(43). This model is integrated into the second stage to ensure the preservation of safe operational conditions within the modern power distribution network. Moreover, similarly to the initial stage's MPDN operational constraints, constraints (44)-(47) are implemented in this stage primarily for power scheduling purposes. They define the feasible ranges for capacitor reactive power, line active and reactive power, while also ensuring the maintenance of MPDN radiality. Additionally, optimal power flow for three-phase unbalanced MPDN, and node balance equations are also integrated and represented in constraints (48)-(52) in in the Appendices Section (Section 9.4).

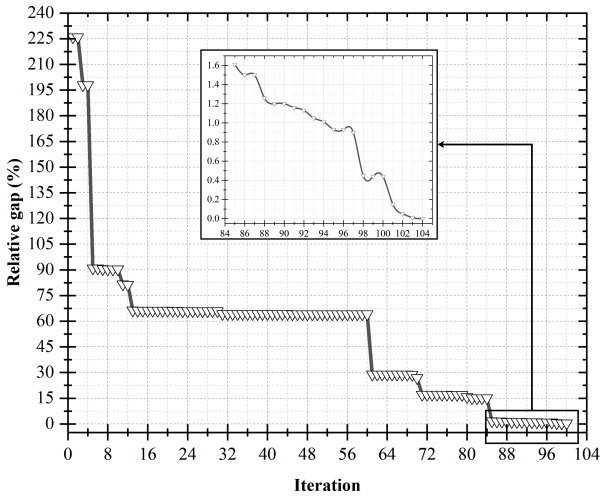

Fig. 4: The relative optimality gap at each iteration.

4 Solution Method

4.1 Rolling Horizon Optimization Framework

Obtaining massive data on EVs and CPs, and the damage status of MPDN components and roads for all time periods of restoration at $t = 0$ is a challenging task [10]. Hence, a rolling optimization framework is adopted to solve the problem recursively in a finite-moving horizon of intervals [40]. The time horizon ($\mathcal{T}$) is discretized into equal time intervals (Δt), and the problem is solved at each interval where $\mathcal{T} = 24$ and $\Delta t = 0.5\ hr$. The decisions and information in the first interval are implemented and updated at each (t), the prediction horizon is shifted forward and the calculation is repeated until the end of the time horizon.

4.2 Linearization Techniques

The critical distance calculation model in (10), and the model of energy consumed during travelling in (12) are nonlinear. Therefore, for constraint (10), α is a large parameter is used to relax this constraint, and the congestion rate variable ($CR^R_{r,t}$) is replaced with a non-constant parameter (CR^R_r), where its value changes over time for each road. Hence, distance calculation model in (10) is reformulated as in constraints (53)-(56) in Appendices Section of the paper (Section 9.5).

Similarly, the travelling energy consumption model in (12) is nonlinear. Thus, it is reformulated and expressed as in (57) by eliminating the travelling status variable ($x^{tr}_{e,t}$) to be maintained in constraint (58) as outlined in Appendices Section of the paper (Section 9.6).

5 Simulation Studies

5.1 Intelligent EVs Coordination Performance

The strategy is implemented in GAMS 42.2.0 studio and solved with Gurobi version 10.0.0 on a PC with a 12th Gen Intel(R) Core(TM) i7-12700k, 3500 MHz CPU processor and 8 GB RAM. The relative optimality gap, a measure of the difference between primal (z_P) and dual (z_D) objective bounds, is defined by the incumbent equation (i.e., $gap = |z_P - z_D| \,/\, |z_P|$) as per [41]. The gap decreases monotonically until it reaches a threshold of 0.001%, indicating an optimal solution. This convergence is demonstrated in Fig. 4, where the optimal strategy is achieved within approximately 40 minutes at iteration number 104.

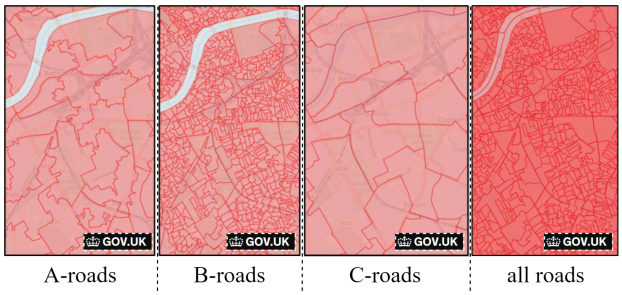

Fig. 5: The map of Battersea road in London, UK; including A-, B-, and C-roads, as well as all roads combined.

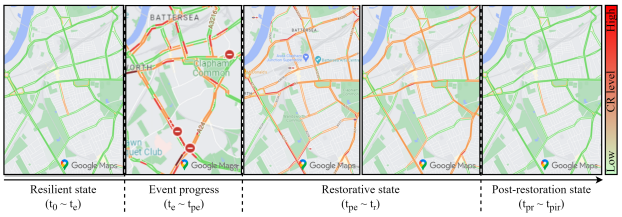

Fig. 6: The map of Battersea road with different congestion rate (CR), ranging from high to low level.

5.2 Case Studies

The application of the aforementioned metric enables the evaluation and comparison of different case studies, elucidating the efficacy of novel and advanced framework elements, such as the prepositioning and dispatching model, information system, integration of ITS/SCS automated system, and geographic graph. These components contribute to achieving an optimal solution and managing the voluminous geographic and technical data associated with roads, MPDN components, CPs, and EVs. Three case studies are designed as follows:

Case-I: presents the proposed methodology.

Case-II: represents a less coordinated approach where the first and second stages are not synchronized to highlight the robustness of the proposed prepositioning model.

Case-III: represents a non-automated EVs dispatching framework to demonstrate the effectiveness of integrating the proposed information system and geographic graph into MPDN resilience-oriented restoration strategies.

5.3 Test Systems

For all three cases, only EVs are considered as mobile power sources to prove the effectiveness of the proposed coordination scheme in handling a large penetration of EVs considering multiple infrastructures. Moreover, a UK-wide map of electric car charging points is adopted from ZAP-MAP [42], as well as real-world EV technical characteristics. The repair time for charging points (CPs) are are coupled with MPDN nodes. A map of Battersea road is used to simulate the transportation system, as shown in Fig. 5. Roads are categorized as A-, B-, and C-roads, which are adopted from the UK Government website [43]. Congestion rates are assigned based on Google Maps colour codes representing live traffic speeds, as in Fig. 6, [44]. The real distances between T-EVs and the associated CPs are adapted with the real traffic information from Google Maps using a Python client [45]. The robustness of the proposed framework is verified on a modified three-phase IEEE 123 node test feeder with the modern power distribution network separated from the main grid during the restoration period ($\mathcal{T} = 24$), where $\Delta t = 0.5\ hr$. MPDN lines repair times are adopted from a two-stage stochastic program proposed in [46] considering the scenario with 15 damaged lines and laterals, as listed in Table 1.

5.4 Simulation Results and Discussion

The proposed pre-positioning model and constrained large-scale EV routing problem are involved in considering several interrelated decision variables, such as the distance travelled by the EVs ($D_{k_\varrho,k_\rho,e,t}$), the energy consumed during travel ($SOC^{tr}_{e,t}$), and the state of charge (SOC) of the EVs upon arrival at charging points ($SOC^{av}_{e,t}$). The optimal values of these variables affect MPDN resilience-oriented restoration strategy. In Fig. 7, the critical path distances ($D_{k_\varrho,k_\rho,e,t}$), and the median value with the normal distribution curve of ($SOC^{tr}_{e,t}$) of each case are illustrated. Owing to the intelligent preparing stage, the proposed novel prepositioning approach has significantly lower values for the distance variable ($D_{k_\varrho,k_\rho,e,t}$). This is due to the coordinated efforts of MPDN operators and automated systems in maximizing $SOC^{av}_{e,t}$ of the EVs, which in turn maximizes the amount of survived loads ($P^L_{l,\phi,t}$) shortly after a rare event. As time passes, the ITS/SCS automated system updates the decision variables obtained in the first stage, and the critical path distance values increase as most of the connected EVs (C-EVs) become discharged (i.e., $SOC^{av}_{e,t} = \underline{SOC}_{e,t}$) and disconnected from charging points, while the travelling EVs (T-EVs) start their journeys to connect to the charging points for discharging.

Traditionally, the optimal solution is typically the one with the lowest distance. However, in the case of the proposed approach (Case-I), while it appears to have the highest distance, ITS/SCS automated system optimizes the distance considering power scheduling constraints, charging point utilization, and overloading and queue management at charging stations. The proposed methodology prioritizes the efficient use of charging points and EVs, taking into account factors such as charging station capacity, battery levels of EVs, and the availability of CPs ensuring that the optimal charging schedule is achieved without causing system overloading or disruptions. Therefore, the proposed methodology is able to optimize distance in a way that reduces $SOC^{tr}_{e,t}$ having a maximum amount of restored loads. As a consequence, Case-I has shown its robustness and resilient as in Fig. 7, where the median amount of consumed energy during travel ($SOC^{tr}_{e,t}$) in Case-I is the lowest, saving more than 20% of ($SOC^{av}_{e,t}$) compared to the comparative cases.

The proposed approach aims to increase ($SOC^{av}_{e,t}$) by maximising the number of communicated EVs in both stages. This leads to a higher communication rate of online EVs (i.e., online EVs refer to the EVs that are able to be communicated by ITS/SCS automated system via roadside unites installed on roads using V2I technology). Thus, around 97%, 86%, and 74% of online EVs are communicated for Case-I, Case-II, and Case-III, respectively. This is achieved by considering the proposed information system which allows for efficient collaboration between the automated system of roads and CPs, enabling the transfer and update of data and decisions obtained at $t = 0$. Therefore, the proposed approach achieves a communication rate that is 11% and 23% higher than Case-II and Case-III, respectively, demonstrating the superiority of the proposed information technology for enhancing the MPDN resilience.

The number of communicated EVs is crucial for improving the MPDN resilience, but not all may participate in the restoration process due to interrelated limitations like charging point capacity, capability, road congestion and status, and the EVs' state of charge levels. Therefore, maximizing the number of participating EVs is a challenging task. Despite this, simulation results indicate that the proposed dynamic approach performs well in worst-case scenarios, where 72% of the communicated EVs are able to participate in Case-I. In contrast, only 52% and 17% of EVs participated

Table 1 The repair times of the damaged lines and laterals [46]

Line	**7-8**	**15-17**	**18-19**	**27-33**	**38-39**
Repair time (Δt)	1.25	2.375	2.625	3.75	4.625
Line	**54-57**	**58-59**	**18-163**	**67-72**	**76-86**
Repair time (Δt)	5	5.25	6.125	8.75	12.75
Line	**91-93**	**93-95**	**105-106**	**113-114**	**150-149**
Repair time (Δt)	13.5	14.875	16.25	16.875	24

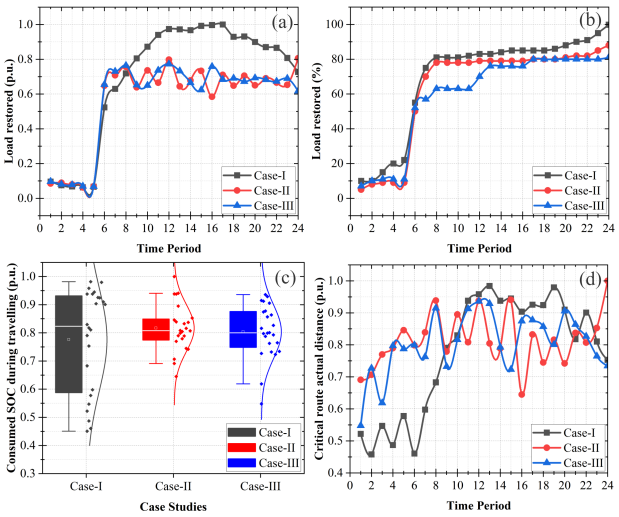

Fig. 7: The simulation results. (a) The load restored at each time step ($P^L_{l,t}$). (b) The commutative load restored at each time step ($\sum_{t\in\mathcal{T}} P^L_{l,t}$). (c) The median and normal distribution curve of consumed SOC during travelling ($SOC^{tr}_{e,t}$). (d) The distance of critical paths ($D_{k_\varrho,k_\rho,r,t}$).

in Case-II and -III, respectively. This demonstrates the robustness of the proposed approach, which intelligently updates and coordinates between MPDN operators and automated systems, resulting in a 20% and 55% increase compared to Case-II and Case-III, respectively, leading to further enhancement of the MPDN resilience.

Fig. 7 presents the load restored at each time step and the cumulative load restored in the presence of the CLPU phenomenon, which can cause delays in the restoration process by absorbing additional power due to undiversified loads ($P^U_{l,\phi,t}$). Case-I, which employs the proposed approach, shows faster and more efficient restoration with higher objective values at all time steps compared to the comparative cases (i.e., Case-II and Case-III). The severe damage scenario assumes that most of the distribution network's 3-phase lines are damaged at $t = 0$, yet the proposed approach still significantly enhances the MPDN resilience by restoring 100% of the load at $t = 24$, which is earlier than the comparative cases. Specifically, Case-II and Case-III restore around 91% and 81% of the load, respectively, at $t = 24$ indicating more EV (i.e., higher amount of SOC), as well as, more time steps are required in comparative cases to fully restore the MPDN.

5.5 Sensitivity Analysis

This section aims to compare the robustness of the prepositioning and routing strategy proposed in this work with the strategy proposed in [11]. To ensure a fair comparison, the test systems and scenarios are correspondingly modified. Thus, Case-IV is added to represent the proposed coordination framework with 6 mobile emergency power sources (including 2 mobile energy storage systems (MESSs), 2 mobile emergency generators (MEGs), and 2 EV fleets). Further, Also, 6 charging stations are placed per [11], and the time window is considered to be $\mathcal{T} = 48$. The involved MEGs are assumed to be three-phase. The result in Fig.8 shows that the proposed method exhibits enhanced MPDN resiliency during the post-event state ($t_{pe} \sim t_{pr}$), with a 14% increase in the amount of survived loads compared to the case in [11]. This is attributed to the well-coordinated efforts of the operators in the pre-event stage ($t_0 \sim t_{pe}$), where the information generated by the automated systems are optimally utilized in solving the pre-positioning, routing and power scheduling problems.

In the restorative state, the routing and dispatching strategy proposed in [11] restored more loads between $t = 5$ and $t = 24$ due to it assuming normal road statuses and neglecting the congestion

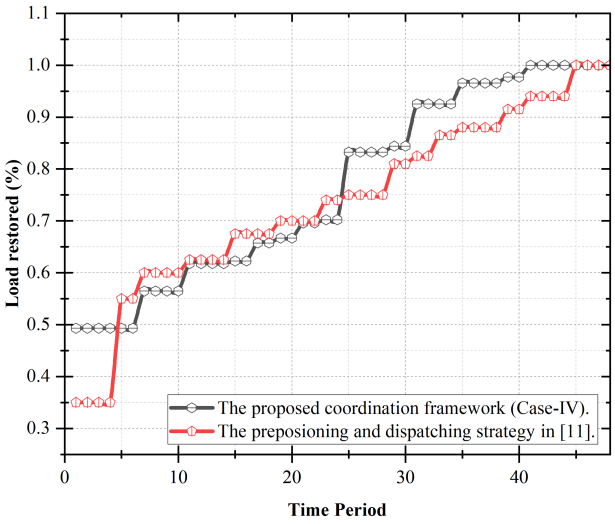

Fig. 8: Restored loads at each time period for the proposed strategy in this work and in [11].

level. In contrast, the proposed strategy experiences delays and critical path damage and closures, which led to longer travel times and distances for some EV fleets and MESS units. On the other hand, the proposed approach in this study exhibits superior performance (i.e., from $t = 25$) when the transportation automated systems report that the roads are restored and repaired. As a result, the proposed strategy allows for more flexible routing of mobile power sources on the road network due to the well-coordinated efforts of the MPDN operators and the ITS/SCS automated systems in the preparation and restoration phases. Hence, the MPDN loads are fully restored at $t = 41$ in Case-IV (i.e., the proposed coordination framework), which is earlier than the work in [11], where it was achieved at $t = 45$.

6 Further Remarks

The necessity of separating the stages in the proposed two-stage optimization framework arises from the adverse consequences that would arise if the stages were combined into a single detailed model. Such integration would result in escalated complexity, posing computational challenges and diminishing tractability. Moreover, the inter-dependencies between the stages may become complected, preventing independent analysis and optimization. Hence, it is vital to maintain the separation of stages to ensure manageable complexity, facilitate efficient computation, and enable independent evaluation.

Furthermore, it is crucial to acknowledge the uncertainties associated with how EV users behave when they are requested to participate in the restoration processes. Future research aims to address these uncertainties technically. The model is aimed to be published to another journal paper.

In addition, while this paper primarily focuses on a large-single area, the proposed EV coordination methodology has the flexibility to be adapted for multiple independent large areas. This can be achieved by partitioning the problem into m number of sub-problems, where m represents the number of areas, each sub-problem can be solved separately and in parallel, utilizing multiple available PCs. This approach enables efficient and simultaneous optimization of the restoration processes across different areas, facilitating expedited decision-making and enhancing overall system performance.

In addressing optimization problems related to multi-dependent large-scale transportation systems, charging points, distribution systems, and a substantial number of electric vehicles (EVs), the authors have achieved significant progress by introducing an optimization clustering technique with novel algorithms. This approach effectively addresses interdependent across multiple large areas, resulting in promising results. Initial findings indicate this technique outperforms commonly used clustering methods, such as the AI-based K-means clustering technique. The authors aim to publish this work in another journal paper.

7 Conclusion

The proposed intelligent EVs coordination framework proves its robustness and superiority in coordinating a large number of EVs, handling a significant amount of spatiotemporal data, and enabling dynamic data exchange to ensure reliable updates of critical information such as EV location, charging status, and power demand. In the first stage, the proposed prepositioning model successfully addresses prepositioning challenges and improves MPDN resilience shortly after the rare event by preserving considerably more energy than in comparative case studies. Also, allowing data transfer to the next stage and applying the proposed information system facilitate communication between ITS/SCS automated system and EVs resulting in achieving a notably higher communication rate than comparative studies. In the second stage, the proposed dispatching approach successfully manages geographical and operational constraints of roads and charging points to control the movement of EVs avoiding long queues and preventing overloading at charging stations. This demonstrates the superiority of the proposed geographic graphs in handling a huge amount of geographical information for improving the routing in the penetration of a large number of EVs resulting in that a significantly higher number of communicated EVs being able to participate in the proposed methodology, compared to comparative case studies.

The proposed intelligent framework outperforms all published studies in the literature in worst-case scenarios where it has successfully proven its ability to fully restore the loads in a much earlier time step. Henceforward, it is crucial for modern power distribution network planners to consider implementing intelligent EV coordination frameworks to enhance resilience-oriented smart restoration strategies in the face of increasing rare events.

Acknowledgment

The authors are grateful to the University of Birmingham for funding this research paper, and acknowledge the financial support from Taibah University, which sponsored author A. Alghamdi.

8 References

1 A. A. M. Alghamdi and D. Jayaweera, "Modelling frameworks applied in smart distribution network resiliency and restoration," in *2022 IEEE 16th International Conference on Compatibility, Power Electronics, and Power Engineering (CPE-POWERENG)*. IEEE, 2022, pp. 1–8.

2 G. Kandaperumal and A. K. Srivastava, "Resilience of the electric distribution systems: concepts, classification, assessment, challenges, and research needs," *IET Smart Grid*, vol. 3, no. 2, pp. 133–143, 2020.

3 A. Hussain, V.-H. Bui, and H.-M. Kim, "Optimal sizing of battery energy storage system in a fast ev charging station considering power outages," *IEEE Transactions on Transportation Electrification*, vol. 6, no. 2, pp. 453–463, 2020.

4 Z. Yang, P. Dehghanian, and M. Nazemi, "Seismic-resilient electric power distribution systems: Harnessing the mobility of power sources," *IEEE Transactions on Industry Applications*, vol. 56, no. 3, pp. 2304–2313, 2020.

5 Y. Wang, Y. Xu, J. Li, C. Li, J. He, J. Liu, and Q. Zhang, "Dynamic load restoration considering the interdependencies between power distribution systems and urban transportation systems," *CSEE Journal of Power and Energy Systems*, vol. 6, no. 4, pp. 772–781, 2020.

6 L. Jiang, X. Li, T. Long, R. Zhou, J. Jiang, Z. Bie, H. Tian, G. Li, and Y. Ling, "Resilient service restoration for distribution systems with mobile resources using floyd-based network simplification method: Resilient service restoration for ds with mobile resources using floyd-based network simplification method," *IET Generation, Transmission & Distribution*, vol. 16, no. 3, pp. 414–429, 2022.

7 B. Li, Y. Chen, W. Wei, S. Huang, and S. Mei, "Resilient restoration of distribution systems in coordination with electric bus scheduling," *IEEE Transactions on Smart Grid*, vol. 12, no. 4, pp. 3314–3325, 2021.

8 M. Nazemi, P. Dehghanian, and Z. Yang, "Swift disaster recovery for resilient power grids: Integration of ders with mobile power sources," in *2020 International Conference on Probabilistic Methods Applied to Power Systems (PMAPS)*. IEEE, 2020, pp. 1–6.

9 B. Li, Y. Chen, W. Wei, S. Huang, Y. Xiong, S. Mei, and Y. Hou, "Routing and scheduling of electric buses for resilient restoration of distribution system," *IEEE Transactions on Transportation Electrification*, vol. 7, no. 4, pp. 2414–2428, 2021.
10 S. Yao, P. Wang, X. Liu, H. Zhang, and T. Zhao, "Rolling optimization of mobile energy storage fleets for resilient service restoration," *IEEE Transactions on Smart Grid*, vol. 11, no. 2, pp. 1030–1043, 2019.
11 S. Lei, C. Chen, H. Zhou, and Y. Hou, "Routing and scheduling of mobile power sources for distribution system resilience enhancement," *IEEE Transactions on Smart Grid*, vol. 10, no. 5, pp. 5650–5662, 2018.
12 P. Zhao, C. Li, Y. Fu, Y. Hui, Y. Zhang, and N. Cheng, "Blockchain-enabled conditional decentralized vehicular crowdsensing system," *IEEE Transactions on Intelligent Transportation Systems*, 2022.
13 R. Zhang, L. Wu, S. Cao, D. Wu, and J. Li, "A vehicular task offloading method with eliminating redundant tasks in 5g hetnets," *IEEE Transactions on Network and Service Management*, 2022.
14 X. Wang, S. Garg, H. Lin, G. Kaddoum, J. Hu, and M. M. Hassan, "Heterogeneous blockchain and ai-driven hierarchical trust evaluation for 5g-enabled intelligent transportation systems," *IEEE Transactions on Intelligent Transportation Systems*, 2021.
15 C. Lei, L. Lu, and Y. Ouyang, "System of systems model for planning electric vehicle charging infrastructure in intercity transportation networks under emission consideration," *IEEE Transactions on Intelligent Transportation Systems*, 2021.
16 S. Turner and S. Uludag, "Towards smart cities: interaction and synergy of the smart grid and intelligent transportation systems," *Smart Grid: Networking, Data Management and Business Models*, 2015.
17 F. Zhu, Z. Li, S. Chen, and G. Xiong, "Parallel transportation management and control system and its applications in building smart cities," *IEEE Transactions on Intelligent Transportation Systems*, vol. 17, no. 6, pp. 1576–1585, 2016.
18 A. A. M. Alghamdi and D. Jayaweera, "Innovative prepositioning and dispatching schemes of electric vehicles for smart distribution network resiliency and restoration," in *2022 IEEE PES 14th Asia-Pacific Power and Energy Engineering Conference (APPEEC)*. IEEE, 2022, pp. 1–6.
19 Y. Xu, Y. Wang, J. He, M. Su, and P. Ni, "Resilience-oriented distribution system restoration considering mobile emergency resource dispatch in transportation system," *IEEE Access*, vol. 7, pp. 73 899–73 912, 2019.
20 S. Afzal, H. Mokhlis, H. A. Illias, N. N. Mansor, and H. Shareef, "State-of-the-art review on power system resilience and assessment techniques," *IET Generation, Transmission & Distribution*, vol. 14, no. 25, pp. 6107–6121, 2020.
21 M. H. Amirioun, F. Aminifar, and H. Lesani, "Towards proactive scheduling of microgrids against extreme floods," *IEEE Transactions on Smart Grid*, vol. 9, no. 4, pp. 3900–3902, 2017.
22 W. Drira, K. Ahn, H. Rakha, and F. Filali, "Development and testing of a 3g/lte adaptive data collection system in vehicular networks," *IEEE Transactions on Intelligent Transportation Systems*, vol. 17, no. 1, pp. 240–249, 2015.
23 S. Zeadally, J. Guerrero, and J. Contreras, "A tutorial survey on vehicle-to-vehicle communications," *Telecommunication Systems*, vol. 73, no. 3, pp. 469–489, 2020.
24 A. R. Khan, M. F. Jamlos, N. Osman, M. I. Ishak, F. Dzaharudin, Y. K. Yeow, and K. A. Khairi, "Dsrc technology in vehicle-to-vehicle (v2v) and vehicle-to-infrastructure (v2i) iot system for intelligent transportation system (its): a review," *Recent Trends in Mechatronics Towards Industry 4.0*, pp. 97–106, 2022.
25 S. Lei, C. Chen, Y. Li, and Y. Hou, "Resilient disaster recovery logistics of distribution systems: Co-optimize service restoration with repair crew and mobile power source dispatch," *IEEE Transactions on Smart Grid*, vol. 10, no. 6, pp. 6187–6202, 2019.
26 Z. Yang, P. Dehghanian, and M. Nazemi, "Enhancing seismic resilience of electric power distribution systems with mobile power sources," in *2019 IEEE Industry Applications Society Annual Meeting*. IEEE, 2019, pp. 1–7.
27 L.-J. Yang, Y. Zhao, C. Wang, P. Gao, and J.-H. Hao, "Resilience-oriented hierarchical service restoration in distribution system considering microgrids," *IEEE Access*, vol. 7, pp. 152 729–152 743, 2019.
28 T. Ding, Z. Wang, W. Jia, B. Chen, C. Chen, and M. Shahidehpour, "Multiperiod distribution system restoration with routing repair crews, mobile electric vehicles, and soft-open-point networked microgrids," *IEEE Transactions on Smart Grid*, vol. 11, no. 6, pp. 4795–4808, 2020.
29 L. Che and M. Shahidehpour, "Adaptive formation of microgrids with mobile emergency resources for critical service restoration in extreme conditions," *IEEE Transactions on Power Systems*, vol. 34, no. 1, pp. 742–753, 2018.
30 B. Taheri, A. Safdarian, M. Moeini-Aghtaie, and M. Lehtonen, "Distribution system resilience enhancement via mobile emergency generators," *IEEE Transactions on Power Delivery*, vol. 36, no. 4, pp. 2308–2319, 2020.
31 W. Wang, X. Xiong, Y. He, J. Hu, and H. Chen, "Scheduling of separable mobile energy storage systems with mobile generators and fuel tankers to boost distribution system resilience," *IEEE Transactions on Smart Grid*, vol. 13, no. 1, pp. 443–457, 2021.
32 B. Chen, Z. Ye, C. Chen, and J. Wang, "Toward a milp modeling framework for distribution system restoration," *IEEE Transactions on Power Systems*, vol. 34, no. 3, pp. 1749–1760, 2018.
33 B. Chen, C. Chen, J. Wang, and K. L. Butler-Purry, "Sequential service restoration for unbalanced distribution systems and microgrids," *IEEE Transactions on Power Systems*, vol. 33, no. 2, pp. 1507–1520, 2017.
34 M. E. Baran and F. F. Wu, "Network reconfiguration in distribution systems for loss reduction and load balancing," *IEEE Transactions on Power delivery*, vol. 4, no. 2, pp. 1401–1407, 1989.
35 M. Baran and F. Wu, "Optimal capacitor placement on radial distribution systems," *IEEE Transactions on Power Delivery*, vol. 4, no. 1, pp. 725–734, 1989.
36 R. R. Gonçalves, J. F. Franco, and M. J. Rider, "Short-term expansion planning of radial electrical distribution systems using mixed-integer linear programming," *IET Generation, Transmission & Distribution*, vol. 9, no. 3, pp. 256–266, 2015.
37 A. Arif, Z. Wang, J. Wang, and C. Chen, "Power distribution system outage management with co-optimization of repairs, reconfiguration, and dg dispatch," *IEEE Transactions on Smart Grid*, vol. 9, no. 5, pp. 4109–4118, 2017.
38 M. Song, W. Sun *et al.*, "Robust distribution system load restoration with time-dependent cold load pickup," *IEEE Transactions on Power Systems*, vol. 36, no. 4, pp. 3204–3215, 2020.
39 C.-C. Liu, V. Vittal, K. Tomsovic, W. Sun, C. Wang, R. Perez, T. Graf, B. Wells, H. Yuan, B. Moradzadeh *et al.*, "Development and evaluation of system restoration strategies from a blackout-final project report," in *Tech. Rep. PSERC Publication 09-08, Power Systems Engineering Research Center, 577*. Engineering Research Center Tempe, 2009.
40 A. O'Connell, D. Flynn, and A. Keane, "Rolling multi-period optimization to control electric vehicle charging in distribution networks," *IEEE Transactions on Power Systems*, vol. 29, no. 1, pp. 340–348, 2013.
41 Gurobi Optimization, LLC, "MIPGap," 2023. [Online]. Available: https://www.gurobi.com/documentation/9.5/refman/mipgap2.html
42 ZapMap, "Map of electric charging points for electric cars uk: Zap-map," *Zap-Map*, 2023. [Online]. Available: https://www.zap-map.com/live/
43 UK.GOV, "Statistical gis boundary files for london," *Find open data*, 2023. [Online]. Available: https://www.data.gov.uk/
44 Google, "Map of london," 2023. [Online]. Available: http://maps.google.co.uk/
45 C. Aybar, Q. Wu, L. Bautista, R. Yali, and A. Barja, "rgee: An r package for interacting with google earth engine," *Journal of Open Source Software*, vol. 5, no. 51, p. 2272, 2020.
46 A. Arif, Z. Wang, C. Chen, and J. Wang, "Repair and resource scheduling in unbalanced distribution systems using neighborhood search," *IEEE Transactions on Smart Grid*, vol. 11, no. 1, pp. 673–685, 2019.
47 A. Borghetti, "A mixed-integer linear programming approach for the computation of the minimum-losses radial configuration of electrical distribution networks," *IEEE Transactions on Power Systems*, vol. 27, no. 3, pp. 1264–1273, 2012.

9 Appendices

9.1 Constraints Associated With The EVs Proactive Prepositioning Model:

The following equations pertain to the proposed proactive prepositioning model of EVs that is outlined in Section 3.1. Constraint (20) represents the radiality constraint, which is derived from reference [47]. Constraints (21) and (22) define the limits for active discharging and charging power of EVs, respectively. Constraint (23) ensures the maintenance of limits for reactive power of a capacitor (v). Constraints (24) and (25) impose restrictions on line active and reactive power, node voltages, and regulator voltages, ensuring their adherence to safe margins.

$$\sum_{ij} x^B_{ij,t} \leq \left|\mathcal{B}^O\right| - 1, \forall ij \in \mathcal{B}^O, t = 0 \tag{20}$$

$$\overline{P}^{disch}_{e,t} x_{e,t} \geq P^{disch}_{e,t} \geq 0, \forall e \in \mathcal{G}^E, t = 0 \tag{21}$$

$$\overline{P}^{ch}_{e,t} x_{e,t} \geq P^{ch}_{e,t} \geq 0, \forall e \in \mathcal{G}^E, t = 0 \tag{22}$$

$$\overline{Q}^C_{v,\phi,t} x^C_{v,\phi,t} \geq Q^C_{v,\phi,t} \geq 0, \forall v \in \mathcal{V}, \phi \in \Phi, t = 0 \tag{23}$$

$$\overline{P}^B_{ij,\phi,t} x^B_{ij,\phi,t} \geq P^B_{ij,\phi,t} \geq \underline{P}^B_{ij,\phi,t} x^B_{ij,\phi,t} \quad ,\forall ij \in \mathcal{B}, \phi \in \Phi, t = 0 \tag{24}$$

$$\overline{Q}^B_{ij,\phi,t} x^B_{ij,\phi,t} \geq Q^B_{ij,\phi,t} \geq \underline{Q}^B_{ij,\phi,t} x^B_{ij,\phi,t} \quad ,\forall ij \in \mathcal{B}, \phi \in \Phi, t = 0 \tag{25}$$

9.2 Constraints Associated With The EVs Spatial-temporal routing model:

The following equations pertain to the proposed spatial-temporal routing model of EVs (i.e., Section 3.2.1). Constraints (26)-(29) ensure EVs do not deviate from their routing plan initiated by ITS/SCS automated system maintaining the start and end intersections, respectively. Constraints (26)-(27) initiate and conclude the optimal path, respectively. Constraint (28) ensures the transportation of EVs among different coordinates satisfies the necessary travel distance by enforcing that the number of incoming and outgoing edges

from a node are equal. Constraint (29) eliminates sub-tours for routes and ensures EV's route is a single and continuous path that visits all the required coordinates.

$$\sum_{k_\varrho} \overleftrightarrow{x}_{k_\varrho,k_\rho,e,t} = 0, \forall (k_\varrho, k_\rho) \in \mathcal{K} \\ , (k_\varrho, k_\rho) : (\gamma, \beta) = \breve{y} : (\gamma, \beta), e \in \mathcal{G}^E, t \in \mathcal{T} \tag{26}$$

$$\sum_{k_\rho} \overleftrightarrow{x}_{k_\varrho,k_\rho,e,t} = 1, \forall (k_\varrho, k_\rho) \in \mathcal{K} \\ , (k_\varrho, k_\rho) : (\gamma, \beta) = \widehat{y} : (\gamma, \beta), e \in \mathcal{G}^E, t \in \mathcal{T} \tag{27}$$

$$\sum_{k_\varrho} \overrightarrow{x}_{k_\varrho,k_\rho,e,t} = \sum_{k_\rho} \overleftarrow{x}_{k_\varrho,k_\rho,e,t}, \forall (k_\varrho, k_\rho) \in \mathcal{K} \\ , (k_\varrho, k_\rho) : (\gamma, \beta) \neq \breve{y} : (\gamma, \beta), k_\rho : (\gamma, \beta) \neq \widehat{y} : (\gamma, \beta) \\ , e \in \mathcal{G}^E, t \in \mathcal{T}, t + \tau \leq \mathcal{T}, \tau \leq t^{tr}_{e,r} \tag{28}$$

$$D_{k_\rho,e,t} = 0 \\ , \forall k_\rho \in \mathcal{K}, k_\rho : (\gamma, \beta) = \breve{y} : (\gamma, \beta), e \in \mathcal{G}^E, t \in \mathcal{T} \tag{29}$$

9.3 Constraints Associated With The EVs Dynamic Power Scheduling model:

The following equations pertain to the proposed dynamic power scheduling model of EVs (i.e., Section 3.2.2). Constraint (30) limits the SOC level of EVs within the feasible range, respectively. Constraints (31)-(32) define the active discharging/charging power limits of EVs, respectively. Constraint (33) guarantees the charging ($x^{ch}_{e,t}$) and discharging ($x^{disch}_{e,t}$) actions are always mutually exclusive states for each EV (e), and if it is not connected to a CP (cp), it can neither charge nor discharge. Also, it ensures each EV is positioned and connected at a CP (cp) that is predetermined by ITS/SCS automated system. Constraint (34) maintains CP connection capability. Constraints (35)-(36) maintain CPs capacity, where the rate of charging demand and feed electricity back into the grid do not exceed the capacity of CPs, respectively.

$$\underline{SOC}_{e,t} \leq SOC^{av}_{e,t} \leq \overline{SOC}_{e,t}, \forall e \in \mathcal{G}^E, t \in \mathcal{T} \tag{30}$$

$$\overline{P}^{disch}_{e,t} x_{e,t} \geq P^{disch}_{e,t} \geq 0, \forall e \in \mathcal{G}^E, t \in \mathcal{T} \tag{31}$$

$$\overline{P}^{ch}_{e,t} x_{e,t} \geq P^{ch}_{e,t} \geq 0, \forall e \in \mathcal{G}^E, t \in \mathcal{T} \tag{32}$$

$$x^{ch}_{e,t} + x^{disch}_{e,t} \leq x_{e,cp,t}, \forall e \in \mathcal{G}^E, cp \in \mathcal{N}^{CP}, t \in \mathcal{T} \tag{33}$$

$$\sum_{e} x_{e,t} \leq x_{cp,t}, \forall e \in \mathcal{G}^E, cp \in \mathcal{N}^{CP}, t \in \mathcal{T} \tag{34}$$

$$0 \leq P^{disch}_{e,t} \leq \overline{P}^{disch}_{cp,t}, \forall e \in \mathcal{G}^E, cp \in \mathcal{N}^{CP}, t \in \mathcal{T} \tag{35}$$

$$0 \leq P^{ch}_{e,t} \leq \overline{P}^{ch}_{cp,t}, \forall e \in \mathcal{G}^E, cp \in \mathcal{N}^{CP}, t \in \mathcal{T} \tag{36}$$

9.4 Constraints Associated With The Operation of Modern Power Distribution Network:

The following equations pertain to the MPDN operational constraints (i.e., Section 3.2.3). Constraints (37)-(43) represent fault location, isolation, and service restoration (FLISR) model which are used to reconfigure the MPDN, isolate the failed lines, and ensure the restored lines cannot be disconnected again [32]. Constraints (37) ensures the voltage limits for MPDN nodes are within the permissible range. Constraint (38) forces the MPDN line with voltage regulators to be within the feasible limits. Constraints (39)-(40) ensure both end nodes of a switchable line must be energized when it is activated. Similarly, Constraints (41)-(42) ensure a non-switchable line is promptly energized when either of its end nodes receives power. Constraint (43) establishes that an energized line cannot be tripped afterwards.

$$\overline{V}_{i,\phi,t} x^N_{i,t} \geq V_{i,\phi,t} \geq \underline{V}_{i,\phi,t} x^N_{i,t}, \forall i \in \mathcal{N}, \phi \in \Phi, t \in \mathcal{T} \tag{37}$$

$$\overline{V}_{ij,\phi,t} x^B_{ij,t} x^V_{v,t} \geq V_{v,\phi,t} \geq \underline{V}_{ij,\phi,t} x^B_{ij,t} x^V_{v,t} \\ , \forall v \in \mathcal{V}, ij \in \mathcal{B} \cap \mathcal{V}, \phi \in \Phi, t \in \mathcal{T} \tag{38}$$

$$x^B_{ij,\phi,t} \leq x^N_{i,\phi,t}, \forall ij \in \mathcal{B}^S/\mathcal{B}^F, \phi \in \Phi, t \in \mathcal{T} \tag{39}$$

$$x^B_{ij,\phi,t} \leq x^N_{j,\phi,t}, \forall ij \in \mathcal{B}^S/\mathcal{B}^F, \phi \in \Phi, t \in \mathcal{T} \tag{40}$$

$$x^B_{ij,\phi,t} = x^N_{i,\phi,t}, \forall ij \in \mathcal{B}/\left\{\mathcal{B}^S \cup \mathcal{B}^F\right\}, \\ \phi \in \Phi, t \in \mathcal{T} \tag{41}$$

$$x^B_{ij,\phi,t} = x^N_{j,\phi,t}, \forall ij \in \mathcal{B}/\left\{\mathcal{B}^S \cup \mathcal{B}^F\right\}, \\ \phi \in \Phi, t \in \mathcal{T} \tag{42}$$

$$x^B_{ij,\phi,t} - x^B_{ij,\phi,t-1} \geq 0, \forall ij \in \mathcal{B}^S/\mathcal{B}^F, \phi \in \Phi, 1 \leq t < \mathcal{T} \tag{43}$$

Also, constraints (44)-(52) are utilized primarily for power scheduling purposes, similar to the operational constraints in the first stage. These constraints define the acceptable ranges for capacitor reactive power (44)-(46), line active and reactive power (46), and radiality of the modern power distribution network (47).

$$\overline{Q}^C_{v,\phi,t} x^C_{v,\phi,t} \geq Q^C_{v,\phi,t} \geq 0, \forall v \in \mathcal{V}, \phi \in \Phi, t \in \mathcal{T} \tag{44}$$

$$\overline{P}^B_{ij,\phi,t} x^B_{ij,\phi,t} \geq P^B_{ij,\phi,t} \geq \underline{P}^B_{ij,\phi,t} x^B_{ij,\phi,t} \\ , \forall ij \in \mathcal{B}, \phi \in \Phi, t \in \mathcal{T} \tag{45}$$

$$\overline{Q}^B_{ij,\phi,t} x^B_{ij,\phi,t} \geq Q^B_{ij,\phi,t} \geq \underline{Q}^B_{ij,\phi,t} x^B_{ij,\phi,t} \\ , \forall ij \in \mathcal{B}, \phi \in \Phi, t \in \mathcal{T} \tag{46}$$

$$\sum_{ij} x^B_{ij,t} \leq \left|\mathcal{B}^O\right| - 1, \forall ij \in \mathcal{B}^O, t \in \mathcal{T} \tag{47}$$

Furthermore, equations (48)-(52) are utilized to enforce constraints in the second stage of the three-phase unbalanced MPDN optimal power flow and node balance equations, respectively.

$$V_{i,\phi,t} - V_{j,\phi,t} \leq \widetilde{z}_{ij,\phi} S^*_{ij,\phi,t} + \widetilde{z}^*_{ij,\phi} S_{ij,\phi,t} \\ + M\left(1 - x^N_{i,\phi,t}\right), \forall ij \in \mathcal{B}/\mathcal{V}, \phi \in \Phi, t \in \mathcal{T} \tag{48}$$

$$V_{i,\phi,t} - V_{j,\phi,t} \geq \widetilde{z}_{ij,\phi} S^*_{ij,\phi,t} + \widetilde{z}^*_{ij,\phi} S_{ij,\phi,t} \\ - M\left(1 - x^N_{i,\phi,t}\right), \forall ij \in \mathcal{B}/\mathcal{V}, \phi \in \Phi, t \in \mathcal{T} \tag{49}$$

$$\left(\underline{V}_{i,\phi,t}\right)^2 V_{i,\phi,t} \leq V_{j,\phi,t} \leq \left(\overline{V}_{i,\phi,t}\right)^2 V_{i,\phi,t} \\ , \forall i, j \in \mathcal{V}, \phi \in \Phi, t \in \mathcal{T} \tag{50}$$

$$\sum_{ji} P^B_{ji,\phi,t} + P^{disch}_{e,\phi,t} = \sum_{ij} P^B_{ij,\phi,t} + P^{ch}_{e,\phi,t} + P^L_{l,\phi,t} \\ , \forall e \in \mathcal{G}^E, \phi \in \Phi, t \in \mathcal{T} \tag{51}$$

$$\sum_{ji} Q^B_{ji,\phi,t} + Q^{disch}_{e,\phi,t} + Q^C_{v,\phi,t} = \sum_{ij} Q^B_{ij,\phi,t} + Q^L_{l,\phi,t} \\ , \forall e \in \mathcal{G}^E, \phi \in \Phi, v \in \mathcal{V}, t \in \mathcal{T} \tag{52}$$

9.5 Linear form of critical distance calculation model:

As outlined in Section 4.2, the relaxed form of the nonlinear critical distance calculation model in equation (10) is represented by the subsequent constraints:

$$\begin{aligned} D_{k_\varrho,k_\rho,e,t} = \sum_{k_\varrho} x_{k_\varrho,k_\rho,e,t} \left(D_{k_\varrho,e,t} + \left(D_{k_\varrho,k_\rho,e,t} CR_r^R \right) \right) \\ ,\forall (k_\varrho,k_\rho) \in \mathcal{K}, (k_\varrho,k_\rho) : (\gamma,\beta) = \breve{y} : (\gamma,\beta) \\ ,e \in \mathcal{G}^E, t \in \mathcal{T}, t+\tau \leq \mathcal{T}, \tau \leq t_{e,r}^{tr}, r \in \mathcal{E} \end{aligned} \tag{53}$$

$$D_{k_\rho,e,t} \leq x_{k_\varrho,k_\rho,e,t}\alpha, \forall k_\varrho, k_\rho \in \mathcal{K}, e \in \mathcal{G}^E, t \in \mathcal{T} \tag{54}$$

$$\begin{aligned} D_{k_\rho,e,t} \leq D_{k_\varrho,e,t} + D_{k_\varrho,k_\rho,e,t} \\ ,\forall k_\varrho, k_\rho \in \mathcal{K}, e \in \mathcal{G}^E, r \in \mathcal{E}, t \in \mathcal{T} \end{aligned} \tag{55}$$

$$\begin{aligned} D_{k_\rho,e,t} \geq D_{k_\varrho,e,t} + D_{k_\varrho,k_\rho,e,t} - \alpha + x_{k_\varrho,k_\rho,e,t}\alpha \\ ,\forall k_\varrho, k_\rho \in \mathcal{K}, e \in \mathcal{G}^E, r \in \mathcal{E}, t \in \mathcal{T} \end{aligned} \tag{56}$$

Constraint (53) represents the mathematical expression used for calculating the critical distance. In order to account for all the critical roads traversed by an an EV (e), constraints (54)-(56) are implemented. These constraints ensure that the distances traveled on critical roads are included in the calculation. To restrict the validity of these constraints to segments associated with the critical routes, a large positive number (α) is carefully enforced and selected.

9.6 Linear form of travelling energy consumption model:

As outlined in Section 4.2, the relaxed form of the nonlinear travelling energy consumption model in equation (12) is represented by the subsequent constraints, where constraint (58) is introduced to enforce EV (e) to be either in a connection mode (C-EV) or a travelling mode (T-EV).

$$\begin{aligned} SOC_{e,t}^{tr} = ECR_e D_{k_\varrho,k_\rho,e,t} \\ ,\forall e \in \mathcal{G}^E, k_\varrho, k_\rho \in \mathcal{K}, k_\varrho : (\gamma,\beta) = \breve{y} : (\gamma,\beta), \\ k_\rho : (\gamma,\beta) = \widehat{y} : (\gamma,\beta), t \leq t^{ar} \end{aligned} \tag{57}$$

$$x_{e,t}^{tr} + x_{e,t} \leq x_{e,cp,t}, \forall e \in \mathcal{G}^E, cp \in \widehat{\mathcal{Y}}, t \in \mathcal{T} \tag{58}$$